Proceedings of the ICBBG2025
2025 International conference on Bio-mediated and Bio-inspired Geotechnics
18-20 May, 2025 | Tempe, Arizona, USA
https://doi.org/10.53243/ICBBG2025-171

Measuring and Modelling Kinetics of CO_2 Hydration Catalysed by Carbonic Anhydrase in Buffered Systems

Raymond Chen[1], Ahmet Mert Kavala[2], Emily Miller[3], Alexandra Clarà Saracho[4], and Ewa J. Marek[5]

[1] Department of Chemical Engineering and Biotechnology, University of Cambridge, Philippa Fawcett Drive, Cambridge, CB3 0AS, United Kingdom; E-mail: rc854@cam.ac.uk
[2] Department of Civil, Architectural and Environmental Engineering, 301 E. Dean Keeton St., ECJ 4.200, Austin, Texas 78712-1700, United States; E-mail: mertkavala@utexas.edu
[3] Department of Civil, Architectural and Environmental Engineering, 301 E. Dean Keeton St., ECJ 4.200, Austin, Texas 78712-1700, United States; E-mail: emilyjmiller@utexas.edu
[4] Department of Civil, Architectural and Environmental Engineering, 301 E. Dean Keeton St., ECJ 4.200, Austin, Texas 78712-1700, United States; E-mail: alexandra.clara.saracho@utexas.edu
[5] Department of Chemical Engineering and Biotechnology, University of Cambridge, Philippa Fawcett Drive, Cambridge, CB3 0AS, United Kingdom; E-mail: ejm94@cam.ac.uk

ABSTRACT

Microbially induced calcium carbonate precipitation (MICP) has been found to accelerate solubility trapping of CO_2, *i.e.* converting labile CO_2(g) to more stable carbonates (HCO_3^-, CO_3^{2-}), mitigating leakage of CO_2 stored in underground sites. MICP is driven by urease and carbonic anhydrase (CA) enzymes, but the impact of CA on the rates of MICP remains largely uncaptured. To study the catalysis by CA, we developed a high-throughput method to determine the rate constants of CA. The pH response of a medium containing CA when subject to a sudden increase in CO_2(aq) concentration was captured experimentally. Subsequently, fitting the input parameters of a modelled pH response to the experiment yielded rate constants of first-order kinetics. Further development of the method will target the determination of the rate constants of reversible Michaelis-Menten kinetics, which are envisaged to help with understanding how CA influences the development of species concentration in MICP over time and if CA can benefit CO_2 trapping with MICP.

INTRODUCTION

Microbially induced calcium carbonate ($CaCO_3$) precipitation (MICP) involves the enzymatic breakdown of urea by ureolytic bacteria, leading to the formation of $CaCO_3$ minerals. MICP has a wide range of application, including mitigating the leakage of CO_2 stored underground, by trapping the stored CO_2 as soluble carbonates (HCO_3^-, CO_3^{2-}) and $CaCO_3$ minerals (Mitchell et al., 2010a). The mechanism of trapping CO_2 works as follows (Konstantinou et al., 2021; Mitchell et al., 2010a; Clarà Saracho and Marek, 2024; Zheng and Qian, 2020): urea is hydrolysed enzymatically by the urease (Ur) enzyme to NH_3 and H_2CO_3, with NH_3 increasing the pH

$$CO(NH_2)_2(aq) + 2\,H_2O \xrightarrow{Ur} 2\,NH_3(aq) + H_2CO_3 \quad (1)$$

$$NH_3(aq) + H_2O \longleftrightarrow NH_4{}^+ + OH^-. \tag{2}$$

A high pH enables the conversion of labile, gaseous $CO_2(g)$ into dissolved carbonates ($HCO_3{}^-$, $CO_3{}^{2-}$), thus capturing some of the $CO_2(g)$ into less labile liquid ions – a process known as solubility trapping. The involved reactions are

$$CO_2(g) \longleftrightarrow CO_2(aq) \tag{3}$$

$$CO_2(aq) + H_2O \xleftrightarrow{CA} H_2CO_3 \tag{4}$$

$$H_2CO_3 \longleftrightarrow HCO_3{}^- + H^+ \tag{5}$$

$$HCO_3{}^- \longleftrightarrow CO_3{}^{2-} + H^+, \tag{6}$$

with the carbonic anhydrase (CA) enzyme capable of catalysing reaction (4). If Ca^{2+} ions are present in the aqueous phase and carbonates are available (concentrations of $HCO_3{}^-$ and $CO_3{}^{2-}$are high at elevated pH, as visible in a Bjerrum plot (Zeebe and Wolf-Gladrow, 2001)), the carbonates can precipitate as $CaCO_3$ mineral, termed mineral trapping, and complete the MICP process by

$$Ca^{2+} + CO_3{}^{2-} \longleftrightarrow CaCO_3(s). \tag{7}$$

Some ureolytic bacteria commonly used for MICP, such as *Sporosarcina pasteurii*, produce both the Ur and CA enzyme. The combined effect of Ur and CA has been studied by Clarà Saracho and Marek (2024), who investigated the Ur and CA gene expression response to the concentration of carbonate species using quantitative polymerase chain reaction (qPCR). Up-regulation of Ur was correlated with high $HCO_3{}^-$ concentration, while CA was found to be up-regulated when the pH was below 7.5, the value associated with the maximum concentration for $HCO_3{}^-$ in a carbon-containing system. Also, higher CA activity was observed at larger $CO_2(g)$ concentrations. Thus, CA was conjectured to be a molecular chaperone in the activation of Ur by controlling the pH to maximise $HCO_3{}^-$ concentration. However, the role of CA in MICP is not fully understood yet.

One approach to understand the effect of CA on the rates in MICP is to model how the catalysis of reaction (4) by CA affects the concentration of species over time, using experimentally determined rate constants for the CA catalysed reaction (4). While rate constants for modelling urease kinetics have been determined (Lauchnor et al., 2015), previous studies on MICP have mostly measured CA activities without determining rate constants. Clarà Saracho and Marek (2024) determined the CA activity colorimetrically with the CA catalysed decomposition of *p*-nitrophenyl acetate. Gilmour et al. (2024) recorded the Wilbur-Anderson Units by measuring the time required for a certain pH decrease from reactions (4), (5) and (6) after introducing $CO_2(aq)$ as substrate. These methods enable a relative comparison of CA activity, but a rate constant of reaction (4) was not obtained. Mirjafari et al. (2007) measured the rate of pH decrease, which is closely related to the $CO_2(aq)$ hydrolysis rate through reactions (4), (5) and (6) if assuming steady state condition. From the rate of pH decrease, the rate constants for non-reversible Michaelis-Menten kinetics were obtained, allowing to model reaction (4) in the forward direction. However, non-reversible Michaelis-Menten kinetics are only suitable for reactions far from equilibrium, *e.g.* in some enzyme assays, while MICP involves reversible mechanisms. Furthermore, the method from Mirjafari et al. (2007) did not consider the effect of buffers in the solution. However, media for growing MICP bacteria can contain buffers in form of amino acids (Thomas et al., 2002). Additionally, buffers are useful or

even necessary for determining the rate of pH decrease, as otherwise, the pH would decrease faster than accurately measurable, reaching equilibrium within ~ 3 s (Mirjafari et al., 2007). In conclusion, we observed the lacking of a simple and reliable method, which is unaffected of buffers in the sample and can obtain rate constants of CA, with which the rate of the catalysed CO_2(aq) hydrolysis reaction (4) can be calculated and not only yield a relative activity of CA.

Therefore, we developed a high-throughput method to quickly obtain all rate constants needed for describing reaction (4) with reversible Michaelis-Menten kinetics, capable of dealing with buffers contained in the sample solution. Mirjafari et al. (2007) monitored the pH change in the CO_2 hydration catalysed by bovine CA using an electrode with a 1-second response time. Studies using pH electrodes reported total reaction volumes of 40 mL (Mirjafari et al., 2007) and 20 mL (Fernández et al., 2018). In our CA assay, only a reduced total reaction volume of 300 µL is required, suitable for a 96-well plate. Using a plate reader, the reaction pH of up to 96 samples could be simultaneously monitored by spectrophotometry with a pH indicator, phenol red, previously employed in the high-throughput measurement of urease enzyme (Okyay and Rodrigues, 2013). Furthermore, accuracy in measuring pH change rates was improved with increased data density with a 0.25-second response time of the used plate reader (Biotek Synergy H1).

We used bovine CA (MP Biomedicals, CAS: 9001-03-0) here for methodology development, because of the ready availability of bovine CA. However, we expect our method to be capable of determining the rate of CO_2(aq) hydration for any type of CA (even beyond MICP), providing the experimental environment of the to be measured CA has a similar pH as our assay (pH 6-8). The rate constants of bovine CA measured in this paper are unsuitable for use in MICP research, as bacterial CA might behave differently. We rather present a high-throughput, low sample volume method for researchers to determine the rate constants of CA for their specific organisms and experiments.

METHODOLOGY

Experimental Determination of pH Change. Enzyme solutions consisting of DI water and bovine CA (MP Biomedicals, CAS: 9001-03-0) in concentrations between 0 and 30 UmL^{-1} (Wilbur-Anderson Units) were prepared. Experiments of each enzyme concentration were done in triplicates in a 96-well plate. The enzyme solution (30 µL) was introduced into a well together with 120 µL phenol red reagent, consisting of 0.025 gL^{-1} phenol red (Sigma-Aldrich, CAS: 143-74-8) in 0.01 M tris buffer (Sigma-Aldrich, CAS: 77-86-1) with pH adjusted to about 8 with HCl. The phenol red was used as an indicator for spectrophotometric measurement of the pH. The prepared plate was placed into a plate reader (Biotek Synergy H1), equipped with a reagent injector module, at 30°C chamber temperature. A CO_2 reagent was prepared by bubbling CO_2(g) at 100 mL min^{-1} through 100 mL DI water for 10 min. At time $t = 0$, 150 µL CO_2 reagent was dispensed into the wells and the absorbance at 560 nm was monitored until $t = 1$ min, ensuring the system has equilibrated. The pH was measured through the absorbance of the phenol red by the plate reader, with the conversion of absorbance to pH determined using a standard curve (Fig. 1), fitted to a logistic function

$$x(\mathrm{pH}) = \frac{a_0}{1 + e^{-a_1(\mathrm{pH} - a_3)}} + a_2, \qquad a_0 = 1.617,\ a_1 = 2.225,\ a_2 = 0.0418,\ a_3 = 8.089 \tag{8}$$

with x the absorption value and a_0, a_1, a_2, a_3 the fitted coefficients. The values for the coefficients in Eq. (8) were obtained from fitting the experimental values in Fig. 1.

Modelling the Concentration of Species. A model for tracking all species participating in the previously described plate reader experiment (*i.e.* CO_2(g), CO_2(aq), H_2CO_3, HCO_3^-, CO_3^{2-}, H^+, OH^-, and tris buffer) was formulated and implemented in Python. The tracking of all species ensured that the influence of buffers on the pH curve and any effects of product saturation are captured. Water as a dominating component in the liquid phase was assumed to be at a constant concentration of 55.5 M and not modelled explicitly. A two phase system was assumed with the well being the liquid phase and the empty space in the plate reader the gaseous phase with a constant atmospheric CO_2(g) concentration of 0.04vol%. Perfect mixing with a uniform distribution of components across the liquid phase was assumed, since the wells are small.

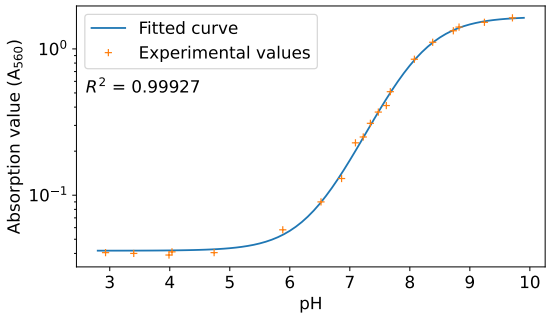

Figure 1. Absorption-pH standard curve.

The species in the plate reader experiment were modelled to react according to reactions (3) - (6) and additionally the alternative paths

$$CO_2(aq) + OH^- \longleftrightarrow HCO_3^- \tag{9}$$

$$HCO_3^- + OH^- \longleftrightarrow CO_3^{2-} + H_2O \tag{10}$$

to reactions (4) - (5), and reaction (6), respectively (Stumm and Morgan, 1996). The tris buffer was assigned the chemical symbol Ba^-, with the conjugate base being HBa. Additional buffers could be included in the model as well. Buffers were modelled to react according to the dissociation reaction

$$HBa \longleftrightarrow Ba^- + H^+. \tag{11}$$

Additionally, the self-ionisation reaction of water was modelled by

$$H^+ + OH^- \longleftrightarrow H_2O. \tag{12}$$

All reactions except reaction (3) took place in the liquid phase, whereas reaction (3) – technically a mass transfer process between the gas and liquid phases – was modelled at the gas-liquid interface. The rate equation describing the mass transfer process (3) was equivalent in form to that of a chemical reaction, but an effective rate constant was applied (Stumm and Morgan, 1996).

The change in species concentrations by the reactions were described by rate equations. For an

example reaction A + B $\overset{k_f}{\underset{k_b}{\longleftrightarrow}}$ C, the rate was described as

$$\frac{d}{dt}[\mathrm{A}] = \frac{d}{dt}[\mathrm{B}] = -\frac{d}{dt}[\mathrm{C}] = -k_f[\mathrm{A}][\mathrm{B}] + k_b[\mathrm{C}] \tag{13}$$

with [A], [B], [C] being the molar concentrations of substances A, B, C, respectively; k_f, k_b the forward and backward reaction rate constants, respectively; and

$$K = \frac{k_f}{k_b} = \frac{[C]}{[A][B]} \tag{14}$$

the equilibrium constant (Mitchell et al., 2010b). The rate equations were implemented as a coupled differential equation system and solved as an initial value problem (ivp) for a system of ordinary differential equations using the dedicated solve_ivp function from scipy (Virtanen et al., 2020). The rate and equilibrium constants used for the rate equations are listed in Table 1.

Table 1. Rate and equilibrium constants of all reactions used to model the plate reader experiment. The values are given at ∼25 °C. The constant concentration of 55.5 M of water was included in the rate and equilibrium constants of H_2O-involving reactions. The first and second dissociation constants of carbonic acid $K_1^* = [\mathrm{HCO_3}^-][\mathrm{H}^+]/[\mathrm{CO_2}(aq)] = 4.47 \cdot 10^{-7}\,\mathrm{M}$ and $K_2^* = [\mathrm{CO_3}^{2-}][\mathrm{H}^+]/[\mathrm{HCO_3}^-] = 4.68 \cdot 10^{-11}\,\mathrm{M}$ and the dissociation constant of water $K_w^* = [\mathrm{H}^+][\mathrm{OH}^-] = 10^{-14}\,\mathrm{M}^2$ were taken from Zeebe and Wolf-Gladrow (2001). The equilibrium constant of reaction (5) was denoted K_5.

Reaction	Forward rate constant k_f	Equilibrium constant $K = \frac{k_f}{k_b}$
Reaction (3)	$2 \cdot 10^{-2}\,\mathrm{s}^{-1}$ (Maier et al., 2004) †	$8.4 \cdot 10^{-1}$ (Sander, 2015)
Reaction (4)	uncatalysed: $4.2 \cdot 10^{-2}\,\mathrm{s}^{-1}$ (fitted)	$K_1^*/K_5 = 2.63 \cdot 10^{-3}$
Reaction (4)	catalysed: fitted	$K_1^*/K_5 = 2.63 \cdot 10^{-3}$
Reaction (5)	$1 \cdot 10^{7}\,\mathrm{s}^{-1}$ (Gibbons and Edsall, 1963)	$K_5 = 1.7 \cdot 10^{-4}\,\mathrm{M}$ (Gibbons and Edsall, 1963)
Reaction (6)	$3\,\mathrm{s}^{-1}$ (Mitchell et al., 2010b)	$K_2^* = 4.68 \cdot 10^{-11}\,\mathrm{M}$
Reaction (9)	$8.5 \cdot 10^{3}\,\mathrm{s}^{-1}\mathrm{M}^{-1}$ (Stumm and Morgan, 1996)	$K_1^*/K_w^* = 4.47 \cdot 10^{7}\,\mathrm{M}^{-1}$
Reaction (10)	$6 \cdot 10^{9}\,\mathrm{s}^{-1}\mathrm{M}^{-1}$ (Stumm and Morgan, 1996)	$K_2^*/K_w^* = 4.68 \cdot 10^{3}\,\mathrm{M}^{-1}$
Reaction (11)	$1 \cdot 10^{10}\,\mathrm{s}^{-1}$ ‡	$8.51 \cdot 10^{-9}\,\mathrm{M}$ Goldberg et al. (2002)
Reaction (12)	$1.4 \cdot 10^{11}\,\mathrm{s}^{-1}\mathrm{M}^{-1}$ (Stillinger, 1978)	$1/K_w^* = 10^{14}\,\mathrm{M}^{-2}$

† based on an experimental value for oxygen transfer in bottles in a shaking incubator (Maier et al., 2004), value only an estimate
‡ rate constant could not be found, thus assumed to be instantaneous

At the start of the simulation, the initial $[\mathrm{H}^+]$ and $[\mathrm{OH}^-]$ concentration were set according to the measured initial pH of the well. Buffers were initialised according to the obtained initial $[\mathrm{H}^+]$ by solving the equation system of mass conservation and thermodynamic equilibrium:

$$[\mathrm{Ba}^-] + [\mathrm{HBa}] = c_{\mathrm{Ba}^-} \tag{15}$$

$$\frac{[\mathrm{H}^+][\mathrm{Ba}^-]}{[\mathrm{HBa}]} = 10^{-pK_{a,\mathrm{Ba}^-}} \tag{16}$$

where $pK_{a,\mathrm{Ba^-}}$ is the acid dissociation constant and $c_{\mathrm{Ba^-}}$ the total molar concentration of the buffer $\mathrm{Ba^-}$. For buffers in the media, $pK_{a,\mathrm{Ba^-}}$ and $c_{\mathrm{Ba^-}}$ could be determined by a titration curve, whereas for the tris buffer in the phenol red reagent, both $pK_{a,\mathrm{Ba^-}}$ and $c_{\mathrm{Ba^-}}$ were known. The simulation was started at $t = -12\,\mathrm{s}$ and at $t = 0$, the $[\mathrm{CO_2(aq)}]$ concentration was suddenly increased to simulate the addition of the $\mathrm{CO_2}$ reagent.

First-Order Kinetics. The rate of the CA catalysed reaction (4) can be described by the Michaelis-Menten kinetics (Mirjafari et al., 2007), which approximates to first order reaction kinetics for low substrate and product concentrations. Before trying to fit the rate constants of the Michaelis-Menten kinetics, we used the model to obtain an effective first-order rate constant of the catalysed reaction (4). A first-order rate constant already allows modelling the effect of CA, although care must be taken for high substrate concentration. The rate of reaction (4) was implemented as

$$\frac{d}{dt}[\mathrm{CO_2}(aq)] = -\frac{d}{dt}[\mathrm{H_2CO_3}] = -k_{f,\,CA}[\mathrm{CO_2}(aq)] + \frac{k_{f,\,CA}}{K_4}[\mathrm{H_2CO_3}] \tag{17}$$

with $k_{f,\,CA}$ the effective forward rate constant of the catalysed reaction (4) and K_4 the equilibrium constant of reaction (4).

Although the same $\mathrm{CO_2}$ reagent was used for all experiments, the value to which the pH dropped to slightly differed between the experiments, without a clear correlation to enzyme concentration (Fig. 2a), and might indicate a slightly different $\mathrm{CO_2(aq)}$ concentration in the $\mathrm{CO_2}$ reagent for each experiment. Possibly, the $\mathrm{CO_2(aq)}$ in the $\mathrm{CO_2}$ reagent outgassed upon contact with air throughout the duration of conducting the experiments, leading to different $\mathrm{CO_2(aq)}$ concentrations. Therefore, the $\mathrm{CO_2(aq)}$ concentration of the $\mathrm{CO_2}$ reagent and the rate constant $k_{f,\,CA}$ were fitted simultaneously by minimising the sum of the squared difference between experimental and simulated pH values using the Nelder-Mead method in scipy (Gao and Han, 2012; Virtanen et al., 2020).

An experiment without CA (enzyme concentration of $0\,\mathrm{U mL^{-1}}$) was conducted to validate the model, as the first-order rate constant for the uncatalysed reaction (4) should be the literature value of 0.03-0.06 $\mathrm{s^{-1}}$ (Stumm and Morgan, 1996; Mitchell et al., 2010b; Mirjafari et al., 2007).

Reversible Michaelis-Menten Kinetics. To consider substrate and product saturation of CA, the rate constants of the reversible Michaelis-Menten kinetics (Cornish-Bowden, 1979)

$$\frac{d}{dt}[\mathrm{CO_2}(aq)] = \frac{-\frac{v_{\max,\,\mathrm{CO_2}}[\mathrm{CO_2}(aq)]}{K_{\mathrm{m,\,CO_2}}} + \frac{v_{\max,\,\mathrm{H_2CO_3}}[\mathrm{H_2CO_3}]}{K_{\mathrm{m,\,H_2CO_3}}}}{1 + \frac{[\mathrm{CO_2}(aq)]}{K_{\mathrm{m,\,CO_2}}} + \frac{[\mathrm{H_2CO_3}]}{K_{\mathrm{m,\,H_2CO_3}}}} \tag{18}$$

need to be obtained, with K_m the Michaelis constant and $v_{\max}$ the maximum (or limiting) rate at saturating substrate concentration. Simply using non-reversible Michaelis-Menten kinetics would not be sufficient for purposes of modelling MICP reactions, as the model should be capable of modelling scenarios involving a (near-) equilibrium of the substrate and product $\mathrm{CO_2(aq)}$ and $\mathrm{H_2CO_3}$, for which non-reversible Michaelis-Menten kinetics would be unsuitable. Using the

Haldane relationship (Cornish-Bowden, 1979), $v_{\mathrm{max,\,H_2CO_3}}$ was eliminated, simplifying Eq. (18) to

$$\frac{d}{dt}[\mathrm{CO_2}(aq)] = \frac{\frac{v_{\mathrm{max,\,CO_2}}}{K_{\mathrm{m,\,CO_2}}}\left(-[\mathrm{CO_2}(aq)] + \frac{[\mathrm{H_2CO_3}]}{K_4}\right)}{1 + \frac{[\mathrm{CO_2}(aq)]}{K_{\mathrm{m,\,CO_2}}} + \frac{[\mathrm{H_2CO_3}]}{K_{\mathrm{m,\,H_2CO_3}}}}, \tag{19}$$

leaving the three parameters $v_{\mathrm{max,\,CO_2}}$, $K_{\mathrm{m,\,CO_2}}$, $K_{\mathrm{m,\,H_2CO_3}}$ to be fitted. For each pH-response curve, the CO_2(aq) concentration of the CO_2 reagent was taken from the previous fit of the first-order rate constant from the same response curve. The fitted first-order rate constant from the experiment without CA was used for the uncatalysed portion of reaction (4), which was modelled as a first-order reaction taking place in parallel to the catalysed portion of reaction (4), described by Eq. (19).

RESULTS

First-Order Kinetics. Selected experimental and corresponding simulated pH response curves are presented in Fig. 2a, showing the model to be capable of recreating the experimental pH curves with first-order enzyme kinetics. Some discrepancies were visible, but could be expected, as first-order kinetics are only an approximation in the low-substrate limit of the Michaelis-Menten kinetics.

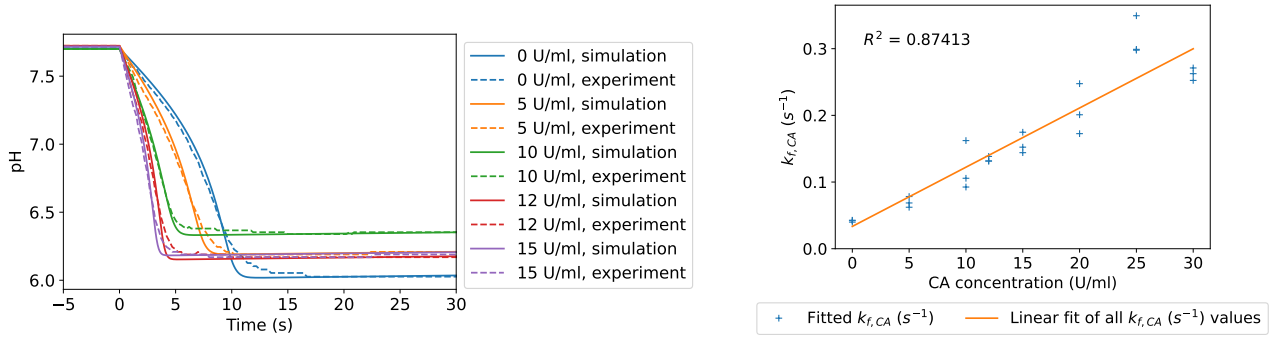

(a) Experimental and simulated curves of pH against time of selected experiments with different enzyme concentrations.

(b) Fitted first-order rate constant $k_{f,\,CA}$ of all experiments.

Figure 2. Fitting the first-order rate constant $k_{f,\,CA}$.

The fitted $k_{f,\,CA}$ of the experiment without CA ($0\,\mathrm{U mL^{-1}}$) had a mean value of $k_{f,\,CA} = 0.042\,\mathrm{s^{-1}}$, agreeing with literature values of 0.03-0.06 $\mathrm{s^{-1}}$ for CO_2 hydrolysis without catalysts (Stumm and Morgan, 1996; Mitchell et al., 2010b; Mirjafari et al., 2007), validating the model.

For the experiments with CA enzyme, a linear relationship between first-order rate constant and enzyme concentration could be expected if assuming low substrate concentrations. For $[\mathrm{CO_2}(aq)] \ll K_{\mathrm{m,\,CO_2}}$ and $[\mathrm{H_2CO_3}] \ll K_{\mathrm{m,\,H_2CO_3}}$, the rate equation (19) of reversible Michaelis-Menten kinetics approximates to the first-order rate equation of

$$\frac{d}{dt}[\mathrm{CO_2}(aq)] = -\frac{v_{\mathrm{max,\,CO_2}}}{K_{\mathrm{m,\,CO_2}}}[\mathrm{CO_2}(aq)] + \frac{v_{\mathrm{max,\,CO_2}}}{K_{\mathrm{m,\,CO_2}} K_4}[\mathrm{H_2CO_3}], \tag{20}$$

where $\frac{v_{\mathrm{max,\,CO_2}}}{K_{\mathrm{m,\,CO_2}}}$ is effectively the first-order rate constant. Since $v_{\mathrm{max,\,CO_2}}$ is proportional to the enzyme concentration (Cornish-Bowden, 1979), the first-order rate constant could be expected

to scale linearly with enzyme concentration, with the intercept equivalent to the first-order rate constant of the uncatalysed reaction (4). The fitted first-order rate constant $k_{f,\,CA}$ of all experiments is plotted in Fig. 2b and indeed, a linear correlation between enzyme concentration and the fitted $k_{f,\,CA}$ is visible, matching the expectation.

Reversible Michaelis-Menten Kinetics. As a further step, the Michaelis-Menten rate constants were fitted to the same pH-curves. Since the Michaelis-Menten kinetics provides a more accurate description of the catalysis by CA than the first-order kinetics, a better fit was expected to be achieved with Michaelis-Menten kinetics. Indeed, the fit obtained using the first-order kinetics can be improved by using reversible Michaelis-Menten kinetics, as the difference between simulated and experimental curve between $t = 0$ and 10 s could be visibly reduced (Fig. 3).

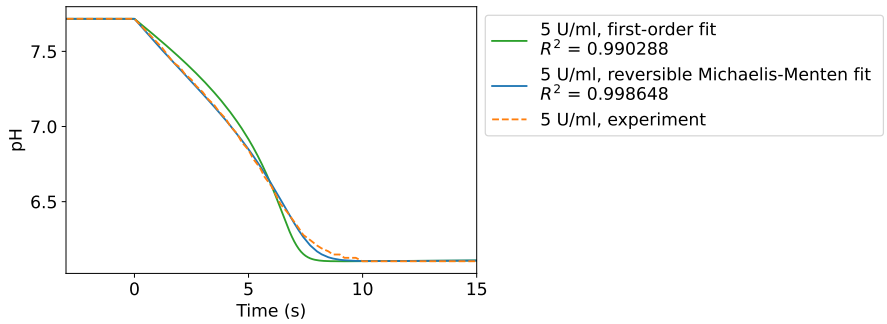

Figure 3. Exemplary comparison of a fit with first-order and reversible Michaelis-Menten kinetics.

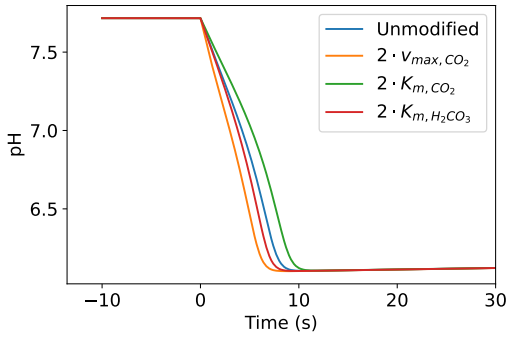

(a) Effect of doubling one of the parameters ($v_{\mathrm{max,\,CO_2}}$, $K_{\mathrm{m,\,CO_2}}$, $K_{\mathrm{m,\,H_2CO_3}}$) used for fitting the pH curve using reversible Michaelis-Menten kinetics.

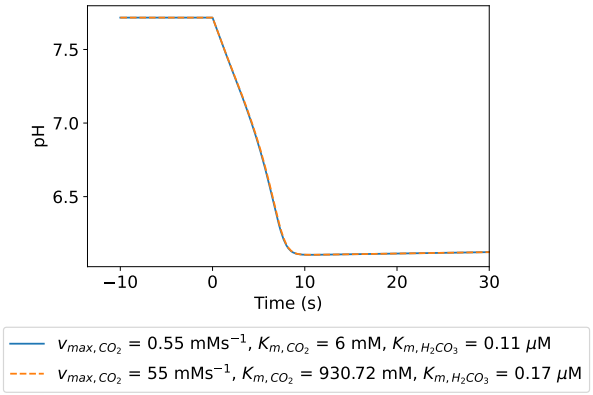

(b) Two different sets of $v_{\mathrm{max,\,CO_2}}$, $K_{\mathrm{m,\,CO_2}}$, $K_{\mathrm{m,\,H_2CO_3}}$ giving indiscernibly similar curves, with the blue curve having the same set as the pH curve in Fig. 3 simulated with reversible Michaelis-Menten kinetics.

Figure 4. Varying the parameters $v_{\mathrm{max,\,CO_2}}$, $K_{\mathrm{m,\,CO_2}}$, $K_{\mathrm{m,\,H_2CO_3}}$.

Furthermore, each of the three to be fitted parameters $v_{\mathrm{max,\,CO_2}}$, $K_{\mathrm{m,\,CO_2}}$, $K_{\mathrm{m,\,H_2CO_3}}$ influence the simulated pH curve. As an example, the reversible Michaelis-Menten fit in Fig. 3 was taken and each of the parameters $v_{\mathrm{max,\,CO_2}} = 0.55\,\mathrm{mMs^{-1}}$, $K_{\mathrm{m,\,CO_2}} = 6\,\mathrm{mM}$, $K_{\mathrm{m,\,H_2CO_3}} = 0.11\,\mu\mathrm{M}$ was

doubled, respectively, to illustrate the effect on the pH curve, as shown in Fig. 4a. Thus, we can confirm that a pH-response curve is influenced by, and contains information about, each of the parameters $v_{\mathrm{max,\,CO_2}}$, $K_{\mathrm{m,\,CO_2}}$, $K_{\mathrm{m,\,H_2CO_3}}$.

However, very different sets of $v_{\mathrm{max,\,CO_2}}$, $K_{\mathrm{m,\,CO_2}}$, $K_{\mathrm{m,\,H_2CO_3}}$ can fit the experimental pH curve similarly well, as exemplarily shown in Fig. 4b. Therefore, simply using a minimising algorithm would not reliably find the correct set of $v_{\mathrm{max,\,CO_2}}$, $K_{\mathrm{m,\,CO_2}}$, $K_{\mathrm{m,\,H_2CO_3}}$ and further research is needed to find the correct set of $v_{\mathrm{max,\,CO_2}}$, $K_{\mathrm{m,\,CO_2}}$, $K_{\mathrm{m,\,H_2CO_3}}$.

CONCLUSION

The effects of CA enzyme on MICP is not fully understood yet. However, determining the CA kinetics is expected to allow precise modelling of the change in species involved in MICP and thus allow to better understand the effects of CA on MICP. Therefore, we developed a high-throughput method requiring minimal sample volume for determining rate constants of CA, based on measuring and modelling the pH response after subjecting the liquid phase to a sudden increase of substrate (CO_2(aq)) concentration. Buffering capacities in the sample liquid can be considered if adding the relevant rate equations of the buffer dissociation reactions. An effective rate constant of CA with first-order kinetics was determined successfully. Fitting rate constants of the reversible Michaelis-Menten kinetics was possible as well, however different sets of rate constants ($v_{\mathrm{max,\,CO_2}}$, $K_{\mathrm{m,\,CO_2}}$, $K_{\mathrm{m,\,H_2CO_3}}$) yielded indiscernibly similar curves. However, the fact that varying any of the three rate constants $v_{\mathrm{max,\,CO_2}}$, $K_{\mathrm{m,\,CO_2}}$, $K_{\mathrm{m,\,H_2CO_3}}$ affected the simulated curve, indicated that determining the rate constants $v_{\mathrm{max,\,CO_2}}$, $K_{\mathrm{m,\,CO_2}}$, $K_{\mathrm{m,\,H_2CO_3}}$ from the pH curve should be possible. Further research will focus on the reason for ambiguous sets of rate constants, so that a fitting method could be developed for reliably determining the rate constants of the reversible Michaelis-Menten kinetics.

SUPPORTING INFORMATION

Depository for model code: `https://github.com/rc854/CO2-Hydration-Kinetics-Model`

REFERENCES

Clarà Saracho, A. and Marek, E. J. (2024). Uncovering the Dynamics of Urease and Carbonic Anhydrase Genes in Ureolysis, Carbon Dioxide Hydration, and Calcium Carbonate Precipitation. *Environmental Science & Technology*.

Cornish-Bowden, A. (1979). Chapter 2 - Introduction to enzyme kinetics. In Cornish-Bowden, A., editor, *Fundamentals of Enzyme Kinetics*, pages 16–38. Butterworth-Heinemann.

Fernández, P. A., Roleda, M. Y., Rautenberger, R., and Hurd, C. L. (2018). Carbonic anhydrase activity in seaweeds: overview and recommendations for measuring activity with an electrometric method, using Macrocystis pyrifera as a model species. *Marine Biology*, 165:1–12.

Gao, F. and Han, L. (2012). Implementing the Nelder-Mead simplex algorithm with adaptive parameters. *Computational Optimization and Applications*, 51(1):259–277.

Gibbons, B. H. and Edsall, J. T. (1963). Rate of hydration of carbon dioxide and dehydration of carbonic acid at 25. *J Biol Chem*, 238(10):3502–7.

Gilmour, K. A., Ghimire, P. S., Wright, J., Haystead, J., Dade-Robertson, M., Zhang, M., and James, P. (2024). Microbially induced calcium carbonate precipitation through CO2 sequestration via an engineered Bacillus subtilis. *Microbial Cell Factories*, 23(1):168.

Goldberg, R. N., Kishore, N., and Lennen, R. M. (2002). Thermodynamic quantities for the ionization reactions of buffers. *Journal of physical and chemical reference data*, 31(2):231–370.

Konstantinou, C., Wang, Y., Biscontin, G., and Soga, K. (2021). The role of bacterial urease activity on the uniformity of carbonate precipitation profiles of bio-treated coarse sand specimens. *Scientific reports*, 11(1):1–17.

Lauchnor, E. G., Topp, D. M., Parker, A. E., and Gerlach, R. (2015). Whole cell kinetics of ureolysis by S porosarcina pasteurii. *Journal of applied microbiology*, 118(6):1321–1332.

Maier, U., Losen, M., and Büchs, J. (2004). Advances in understanding and modeling the gas–liquid mass transfer in shake flasks. *Biochemical Engineering Journal*, 17(3):155–167.

Mirjafari, P., Asghari, K., and Mahinpey, N. (2007). Investigating the application of enzyme carbonic anhydrase for CO2 sequestration purposes. *Industrial & engineering chemistry research*, 46(3):921–926.

Mitchell, A. C., Dideriksen, K., Spangler, L. H., Cunningham, A. B., and Gerlach, R. (2010a). Microbially enhanced carbon capture and storage by mineral-trapping and solubility-trapping. *Environmental science & technology*, 44(13):5270–5276.

Mitchell, M. J., Jensen, O. E., Cliffe, K. A., and Maroto-Valer, M. M. (2010b). A model of carbon dioxide dissolution and mineral carbonation kinetics. *Proceedings of the Royal Society A: Mathematical, Physical and Engineering Sciences*, 466(2117):1265–1290.

Okyay, T. O. and Rodrigues, D. F. (2013). High throughput colorimetric assay for rapid urease activity quantification. *Journal of microbiological methods*, 95(3):324–326.

Sander, R. (2015). Compilation of Henry's law constants (version 4.0) for water as solvent. *Atmospheric Chemistry and Physics*, 15(8):4399–4981.

Stillinger, F. H. (1978). Proton transfer reactions and kinetics in water. *Theoretical chemistry: advances and perspectives*, 3:177–234.

Stumm, W. and Morgan, J. J. (1996). *Aquatic chemistry: chemical equilibria and rates in natural waters, 3rd edition*. John Wiley & Sons.

Thomas, K., Hynes, S., and Ingledew, W. (2002). Influence of medium buffering capacity on inhibition of Saccharomyces cerevisiae growth by acetic and lactic acids. *Applied and environmental microbiology*, 68(4):1616–1623.

Virtanen, P., Gommers, R., Oliphant, T. E., Haberland, M., Reddy, T., Cournapeau, D., Burovski, E., Peterson, P., Weckesser, W., Bright, J., et al. (2020). SciPy 1.0: Fundamental Algorithms for Scientific Computing in Python. *Nature methods*, 17(3):261–272.

Zeebe, R. E. and Wolf-Gladrow, D. (2001). *CO2 in seawater: equilibrium, kinetics, isotopes*. Number 65. Gulf Professional Publishing.

Zheng, T. and Qian, C. (2020). Influencing factors and formation mechanism of CaCO3 precipitation induced by microbial carbonic anhydrase. *Process Biochemistry*, 91:271–281.